Vibrational modes and local order in permanently densified silica glasses: Femtosecond and Raman spectroscopy study

J. Burgin,[1] C. Guillon,[1] P. Langot,[1] and F. Vallée[1,2]
[1]*Centre de Physique Moléculaire Optique et Hertzienne, Université Bordeaux I–CNRS, 351 cours de la Libération, 33405 Talence, France*
[2]*FemtoNanoOptics group, LASIM, Université Lyon I–CNRS, 43 Bd. du 11 Novembre, 69622 Villeurbanne, France*

B. Hehlen[3] and M. Foret[3]
[3]*Laboratoire des Colloïdes, Verres et Nanomatériaux, Université Montpellier II–CNRS, 34095 Montpellier Cedex 5, France*
(Received 26 June 2008; revised manuscript received 21 October 2008; published 17 November 2008)

The D_1 and D_2 vibrational ring modes of normal and densified silica are investigated using a time resolved pump-probe technique and spontaneous Raman spectroscopy. The vibrational response function of both techniques is derived and compared to the experimental results obtained on three samples of silica of increasing density. Comparison of the amplitudes of the time- and frequency-domain responses reveals a much larger increase in concentration of three-membered rings as compared to four-membered ones upon densification. In addition, measurements of the Raman-scattering intensity in SiO_2 also provide a mean to identify bending motions and to estimate the variation of the average Si-O-Si bond angle in densified samples.

DOI: 10.1103/PhysRevB.78.184203 PACS number(s): 78.47.−p, 78.30.Ly, 63.50.−x

I. INTRODUCTION

The structural properties of glasses have been topics of intense theoretical and experimental research over the last decades. This was motivated both by fundamental and technological interest. In this context, the vibrational properties, reflecting the atomic scale structure of materials, constitute an important source of information. Spontaneous Raman-scattering spectroscopy has emerged as a central tool for the investigation of amorphous materials. Such Raman spectra consist primarily of broad structures, generally associated with the vibrational density of states and whose width reflects the structural disorder.[1,2] However, many vitreous materials also exhibit narrow line signatures of local order at the atomic scale. This is for instance the case for vitreous silica whose Raman spectrum shows two sharp lines, known as the D_1 and D_2 defect or ring modes.[3,4] They have been ascribed to the breathing vibrations of the oxygen atoms in local ordered structures formed by four- and three-membered SiO_2 quasiplanar rings, respectively.[2,5–9] These rings have the formula $(\text{-Si-O-})_n$ with $n=3$ or 4. Each Si has two further bonds outside the ring, while the O is only bonded within it. The spectral sharpness is a consequence of the decoupling of the oxygen movement from the other vibrations. The quasiplanar structure of the rings also limits inhomogeneous broadening effects.[4,10] Investigation of the ring-mode evolution under different constraints, such as densification or irradiation, is of central interest for analyzing the induced modification on the local structure. This is particularly interesting in the context of optical damage and predamage studies for analyzing the underlying light induced structural changes and microscopic mechanisms at their origin.[11,12]

Because of their spectral overlap with the broad disorder-associated lines, such precise investigation is sometimes difficult using frequency resolved techniques. This is in particular the case in densified silica where densification increases the spectral overlap of the D_1 line with the broadband R-band produced by oxygen-atom oscillations in the disordered network. This limitation can be circumvented using time-resolved Raman techniques. These have been extensively used to study the vibrational response of matter but little applied to amorphous materials, probably because of their very weak response.[13–17] Time-resolved investigation of the vibrational response of glasses has been recently demonstrated using impulsive-stimulated Raman scattering (ISRS).[18,19] In this technique a vibrational mode is impulsively excited by an optical pulse shorter than its period. Its oscillation is subsequently probed in the time-domain using a second time-delayed pulse yielding information on its period and damping.[15–17] In these measurements, narrow lines of long decay time dominate the long-time scale and can thus be selectively addressed. Exploiting this time-windowing, sharp lines embedded in a broadband can be investigated, making time- and frequency-resolved experiments very complementary.

In this paper we investigate the impact of densification on the vibrational modes of silica using ISRS and spontaneous Raman scattering. Densification does not essentially alter the basic unit, i.e., the SiO_4 tetrahedron, but it changes the medium range glass structure and modifies the bondings in the network. It thus translates into changes of the low and medium frequency vibrational modes involving substructures larger than the tetrahedron such as the ring modes. The induced frequency shifts and line broadenings have already been studied in Raman scattering in the spectral region dominated by oxygen bending motion. However, no information has been reported on the amplitude evolution or on the precise behavior of the ring modes, in particular for D_1. We focus here on an analysis of modifications in the D_1 and D_2 ring-mode characteristics upon densification, comparing the results obtained by femtosecond ISRS and spontaneous Raman spectroscopy. In particular, the determination of the amplitude of the ring-mode responses reveals the evolution of the ring concentration upon densification.

II. EXPERIMENTAL TECHNIQUE

A. Femtosecond ISRS and spontaneous Raman scattering

The time-resolved experiments were performed using femtosecond impulsive-stimulated Raman scattering in the pump-probe configuration.[20,21] The latter can be described as a sequential interaction of two pulses of duration τ_L much shorter than the period of a vibrational mode $T_0=2\pi/\omega_0$. The first pulse launches the mode oscillation whose temporal evolution is monitored by the second time-delayed one. Assuming a single homogeneously broadened mode, described by an assembly of independent harmonic oscillators of number density N_0, displacement amplitude Q, and effective mass μ_0, the excitation process is described by:[14,22–24]

$$\frac{d^2Q}{dt^2}+\frac{2}{T_2}\frac{dQ}{dt}+\omega_0^2Q=\frac{1}{2\mu_0}\left(\frac{\partial\alpha}{\partial Q}\right)_0 EE^*. \tag{1}$$

T_2 is the mode dephasing time, α is the relevant component of the Raman polarizability tensor, and E is the pump-pulse electric field. Similarly, the probe-pulse interaction with the vibrational mode can be described by the application of a force on each oscillator. Depending on the pump-probe delay, it either increases or decreases the coherent vibrational amplitude. Consequently, the probe pulse loses or gains energy from the vibration, respectively, i.e., Stokes or anti-Stokes scattering takes place. For pump-probe delay, t_D, larger than τ_L, the relative change of the total energy $\Delta U^{\mathrm{ho}}/U(t_D)$ of the probe pulse detected after the sample is given by[16,17]

$$\frac{\Delta U^{\mathrm{ho}}}{U}=\frac{4\pi^2U_p}{c^2n^2}\frac{N_0}{\mu_0}\left(\frac{\partial\alpha}{\partial Q}\right)_0^2 L[f(\omega_0)]^2e^{-t_D/T_2}\cos(\omega_0t_D), \tag{2}$$

where L is the interaction length of the beams, U_p the pump-pulse fluence, and n is the sample refractive index at the assumed identical pump and probe wavelength. $f(\omega_0)$ is the excitation function at frequency ω_0,

$$f(\omega_0)=\int_{-\infty}^{+\infty}|I_p(t)|\cos(\omega_0t)dt/U_p, \tag{3}$$

where $I_p(t)$ is the pump-pulse intensity, taken to be symmetric and centered at $t=0$. It reflects the amplitude of the excitation for a given pulse duration τ_L, i.e., the pulse spectral content, the same pump, and probe pulses being assumed. For a short pulse duration, $\omega_0\tau_L\ll1$, the f function is independent of ω_0 and all the modes below and around this frequency are similarly excited and probed. The probe-pulse energy transmitted by the sample exhibits oscillations with the mode period T_0 and an amplitude decaying with the mode dephasing time T_2. These two parameters can thus be precisely determined.

From a general point of view, the time-domain ISRS response is related to the spontaneous Raman spectra for parallel polarization (HH) configuration by Fourier transformation.[23] The former is proportional to the time correlation function of the vibrational mode amplitude Q and the latter to its Fourier transform. For a single homogeneous mode at frequency ω_0 the Raman-scattering intensity in terms of the Raman shift $\omega=\omega_L-\omega_S$ is given by[25,26]

$$I_{\mathrm{RS}}^{\mathrm{ho}}(\omega)=I_{\mathrm{RS}}^{\mathrm{int}}(\omega_0)\frac{1/\pi T_2}{(\omega-\omega_0)^2+(1/T_2)^2}, \tag{4}$$

where $I_{\mathrm{RS}}^{\mathrm{int}}$ is the Raman intensity integrated over the line profile

$$I_{\mathrm{RS}}^{\mathrm{int}}(\omega_0)\propto\frac{\omega_L\omega_S^3}{\omega_0}\frac{N_0}{\mu_0}\left(\frac{\partial\alpha}{\partial Q}\right)_0^2[n_B(\omega_0)+1]V_SI_L. \tag{5}$$

Here, ω_L and I_L are the laser frequency and intensity, respectively, V_S is the fraction of the scattered light analyzed by the spectrometer, and $n_B(\omega_0)$ is the Bose factor at the vibration frequency ω_0. For a narrow line ($\omega_0T_2\ll1$) the time domain signal [Eq. (2)] is then directly proportional to the Fourier transform of $\omega_0I_{\mathrm{RS}}^{\mathrm{ho}}/\omega_S^3[n_B+1]\propto I_{\mathrm{RS}}^{\mathrm{ho}}$.

Owing to the structural disorder, the vibrational modes of glasses are usually distributed in frequency. This leads to a large inhomogeneous broadening of the Raman line whose lineshape reflects the vibrational density of states of the mode rather than the dephasing rate of each component. For a single inhomogeneously broadened line described by an assembly of oscillators with total density N and a Gaussian distribution of their frequency ω, centered at ω_0 with full width at half maximum γ_0, the scattering intensity is given by

$$I_{\mathrm{RS}}(\omega)\propto\frac{I_{\mathrm{RS}}^{\mathrm{int}}(\omega_0)}{\gamma_0}\exp\left(-4\ln(2)\frac{(\omega-\omega_0)^2}{\gamma_0^2}\right), \tag{6}$$

where γ_0 is assumed small compared to ω_0, which is the case for the investigated D_1 and D_2 lines of silica. The homogeneous width of each line component is neglected and its contribution is assumed to be proportional to the individual area with the same Raman susceptibility.

In the time domain, the components of an inhomogenous line are simultaneously excited and detected. The corresponding signal is given by the sum of their contributions,

$$\frac{\Delta U^{\mathrm{inh}}}{U}(t_D)=\frac{\Delta U^{\mathrm{ho}}}{U}(t_D)\exp(-t_D^2/\tau_0^2), \tag{7}$$

where γ_0 is assumed to be sufficiently small (i.e., $\gamma\tau_L\ll1$) to neglect dispersion of the excitation function f over the width of the line. As expected, it is proportional to the Fourier transform of $\omega_0I_{\mathrm{RS}}/\omega_S^3[n_B+1]\propto I_{\mathrm{RS}}$. The different components of the line, initially excited in phase by the pump pulse, drift out of phase with time and eventually destructively interfere. It leads to an additional decay of the time-domain oscillation with an effective decay time $\tau_0=4\sqrt{\ln(2)}/\gamma_0$, directly related to the inhomogeneous linewidth γ_0. In the following, this contribution will be assumed to be much larger than the homogeneous decay ($T_2\gg1/\gamma_0$) that will be neglected.

If i inhomogeneously broadened lines of mean frequency ω_i contribute to the signal, the change in the probe-pulse energy is given by

$$\frac{\Delta U^{\text{inh}}}{U}(t_D) = \frac{\rho}{n^2}\sum_i \mathcal{A}_i \exp(-t_D^2/\tau_i^2)\cos(\omega_i t_D), \tag{8}$$

where ρ is the material density, and N_i is assumed to be proportional to ρ, with $N_i=\beta_i\rho$. $\mathcal{A}_i$ is the density- and index-normalized amplitudes in the time domain for the ith line,

$$\mathcal{A}_i = \frac{4\pi^2}{c^2} L U_p f^2 \frac{\beta_i}{\mu_i}\left(\frac{\partial\alpha}{\partial Q}\right)_i^2 \propto \frac{\omega_i}{\omega_S^3}\frac{1}{\rho V_S}\frac{I_{\text{RS}}^{\text{int}}(\omega_i)}{[n_B(\omega_i)+1]}. \tag{9}$$

It is related to the integrated intensity over the ith line of the imaginary part of the normalized Raman susceptibility

$$\chi_{\text{Norm}} = \frac{1}{\rho V_S}\frac{I_{\text{RS}}(\omega)}{[n_B(\omega)+1]}. \tag{10}$$

For the D_1 and D_2 lines of silica, the variation with pressure of ω_i/ω_S^3 in Eq. (9) can be neglected. $\mathcal{A}_i$ is thus directly proportional to the integrated normalized Raman intensity permitting comparison of the time- and frequency-domain experiments.

B. ISRS experimental setup

The femtosecond experimental setup uses a homemade Ti-sapphire oscillator delivering 15 fs pulses of central wavelength $\lambda_{\text{IR}}\approx 860$ nm and spectral bandwidth of 90 nm FWHM or about 1.2×10^3 cm^{-1}. The output pulse train is separated into two parts to create the pump and probe beams. The two linearly cross-polarized beams are focused into the sample with a 5 cm focal length achromat, the beams making an angle of about 1°. The sizes and spatial overlap of the focal spots are monitored by imaging the sample surface with a microscope and a charge coupled device (CCD) camera. This ensures that measurements are performed in the same conditions in the different samples so that the response amplitudes can be quantitatively compared. The pump-probe delay is controlled by modifying the probe-beam path using a corner cube on a translation stage of 0.125 μm step. The pump beam is mechanical chopped at 1.5 kHz. After spatial and polarization selections, the probe-beam energy transmitted by the sample is detected by a photodiode. The pump induced change of the probe transmission, $\Delta T/T=\Delta U/U$, is monitored using lock-in and differential detection. Taking advantage of the high stability and high repetition rate (80 MHz) of our setup, very high sensitivity $\Delta T/T$ measurements are achieved with a noise level in the 10^{-7} range.

C. Raman experimental setup

The Raman spectra are measured using an argon laser emitting at the wavelength $\lambda=514.5$ nm. The light is analyzed in a backscattering configuration with a Jobin-Yvon T64000 triple-grating spectrometer used in its micromode. The incoming and scattered light are focused and collected with a microscope objective of ×50 magnification, leading to a ~1 μm diameter focal spot and a length of the focal region of a few micometer. The spectral resolution is about 1 cm^{-1} for an entrance slit of 100 μm. Special care is taken to obtain reliable relative intensities of the Raman lines in different samples. For this purpose, the microscope mounted on the spectrometer is used to select the cleanest region of the sample and to precisely focus the laser beam on its entrance surface. The focusing objective is then translated toward the sample, adjusting the focal plane position at a depth of 150 μm from the surface. Owing to the very good optical quality of our samples, this ensures a better than 5% accuracy on relative Raman intensities.

D. Silica samples

High purity silica samples with less than 2 ppm of water are used (Suprasil F300). Densification was achieved by heating to ~1000 K and cooling down to room temperature under hydrostatic pressure in a multianvil high-pressure apparatus.[27] This produced permanently densified silica, d-SiO_2, whose density ρ depends on the temperature-pressure cycle. We use two samples of densities $\rho=2.43$ g/cm^3 and $\rho=2.63$ g/cm^3, plus a normal silica v-SiO_2, with $\rho=2.20$ g/cm^3. The spatial homogeneity of the density of the d-SiO_2 samples, $\Delta\rho/\rho\simeq 1\%$, was measured by high-resolution Brillouin scattering experiments. This ensures that the broadening of the Raman modes is not associated with density fluctuations. The three samples are about 2 mm thick with very good optical quality. Their surfaces were optically polished with diamond paste of 1 μm grain size. The refractive indices of the samples measured with an Abbe refractometer are, in order of increasing densities, $n=1.4616$, $n=1.508$, and $n=1.548$, at $\lambda=514.5$ nm.[28]

III. RAMAN-SCATTERING MEASUREMENTS

Numerical simulations[29] and neutron-diffraction experiments[27] have shown that the mean intertetrahedra Si-O-Si angle and the Si-Si distance decrease upon densification while the regularity of the SiO_4 tetrahedra is barely affected. Compaction of the Si-O-Si network mostly modifies the structural order at the medium range scale, i.e., involving substructures larger than a tetrahedron. In the Raman spectrum these vibrational modes are associated with frequencies below ~650 cm^{-1}. They correspond to the boson peak at low frequency, the broad R band centered around 440 cm^{-1} in v-SiO_2, and the D_1 and D_2 ring modes (Fig. 1). The boson peak is mainly associated with librational-translational motions of rigid SiO_4 tetrahedral.[30,31] Depending on the technique, spectroscopies may be more sensitive to the librational component or to the translational one. For example Raman will not detect *pure* librations of rigid SiO_4 while those are strongly active in hyper-Raman.[30] The R band is due to bending motions of oxygen atoms in Si-O-Si linkages[32] such as in large rings formed by more than four SiO_2.[4] The wide spread in the Si-O-Si angle of the latter translates into a large frequency distribution of the corresponding modes and thus in a large inhomogeneous broadening of the R band.

The normalized Raman susceptibilities [Eq. (10)] measured in the three vitreous silica samples are shown Fig. 1. I_{RS} directly results from the measurement and it is normalized between the different samples taking into account their

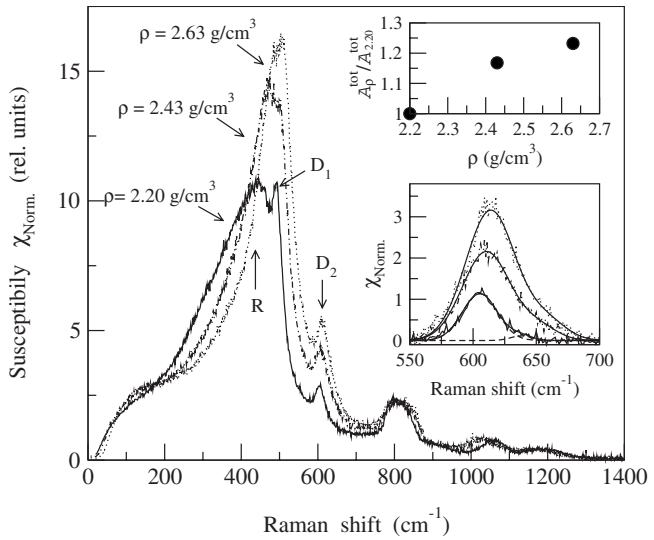

FIG. 1. Normalized Raman susceptibility [Eq. (10)] in relative units for the three silica glasses. The upper inset shows the relative Raman area, $\mathcal{A}_\rho^{\mathrm{tot}}/\mathcal{A}_{2.20}^{\mathrm{tot}}$, which increases in the two densified glasses relative to v-SiO_2. The lower inset shows the spectra of the D_2 lines after subtraction of the tails of the R and D_1 components. The full lines are fits to a sum of a strong and a weak (dashed line) Gaussian functions.

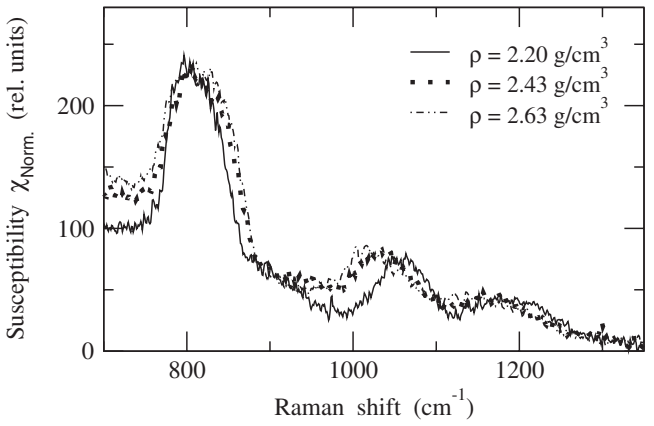

FIG. 2. Raman susceptibility spectra from the high-frequency modes in v-SiO_2 and d-SiO_2 in relative units.

different refractive indices. The concomitant change of the scattering volume modifies I_{RS} by less than 1% and it can be neglected. Upon densification, a large modification of the Raman spectrum is observed with an increase in the normalized susceptibility spectrum mainly in the region of the R band. The structural modification induced by densification does not affect significantly the number of degrees of freedom per unit mass. Thus, one can reasonably assume that the integrated vibrational density of states remains constant from glass to glass. Using the Raman intensity for a vibrational density of states $g(\omega)$,[33]

$$I_{\mathrm{RS}}(\omega) = C(\omega)(n_B + 1)g(\omega)/\omega, \tag{11}$$

where $C(\omega)$ is the Raman coupling coefficient, the total amplitude of the normalized Raman spectra

$$\mathcal{A}_\rho^{\mathrm{tot}} = \frac{1}{\rho V_S}\int \frac{I_{\mathrm{RS}}(\omega)}{[n_B(\omega)+1]}\frac{\omega}{\omega_S^3}d\omega, \tag{12}$$

should be conserved. The variation in $\mathcal{A}_\rho^{\mathrm{tot}}$ relative to normal silica is shown in the upper inset of Fig. 1. Assuming that the integrated $g(\omega)$ is constant, the observed increase mainly arises from a change in $C(\omega)$. For O-bending motions, the intensity is related to the Si-O-Si bond angle θ in v-SiO_2 by $\mathcal{A} \propto \cos^2(\theta/2)$.[8] The 26% increase in $\mathcal{A}_{2.63}^R/\mathcal{A}_{2.20}^R$ extracted experimentally for the R band between 100 and 700 cm^{-1} can thus be explained by a reduction of nearly to 4°–5° of the Si-O-Si average angle in our most densified sample. This value is consistent with theoretical prediction, being in between the 3° obtained from classical molecular dynamics[29] and the 8° extracted from more recent *ab initio* calculations.[34] Similarly, the 18.5% increase of the R band in the sample of density ρ=2.43 $\mathrm{g/cm}^3$ leads to a Si-O-Si average angle reduction in 3°–4° relative to normal silica.

The band at ~805 cm^{-1} and the doublet around 1100 cm^{-1} are less affected by densification (Fig. 2). After subtraction of the background, the normalized areas calculated with Eq. (12) show an increase of 13% and a constant value, respectively, when ρ increases from 2.20 to 2.63 $\mathrm{g/cm}^3$. This different behavior is consistent with the different nature of the modes. The R band corresponds to bending motions more sensitive to reduction of the Si-O-Si bond angle. In contrast, the 805 cm^{-1} structure is associated to both local bending and stretching motions, and a pure stretching for the high-frequency doublet involving either the Si-O-Si bonds[35,36] or SiO_4 tetrahedral.[36,37] The constant area of the high-frequency doublet probably indicates that it is rather associated to quasilocal SiO_4 tetrahedra motions, while its frequency depends on the coupling with the network.

Interestingly, the peak maximum of the 805 cm^{-1} band happens not to depend on density. This will provide an empirical but accurate way to normalize the Raman spectra of densified silicas of poor optical quality, e.g., for Raman microcartography of indented surfaces.[38] This would lead to a more correct intensity normalization compared to arbitrarily adjusting on the maximum of the R band as done in some previous studies. It is also worth noting that the behavior of the 805 cm^{-1} mode under hydrostatic pressure is almost fully reversible even for pressures that induce permanent densification.[39] It strongly hardens under pressure while it only exhibits a broadening on its high-frequency side after the pressure is released in the densified state, as shown in Ref. 40 and in the present work (Fig. 2). This shows that this peak is strongly sensitive to the elastic behavior of silica, and that its broadening in the densified glass can be associated to a redistribution of the elastic strain field.

To better characterize the three membered-ring mode D_2, its lineshape has been extracted by subtraction of the background arising from the R and D_1 components (lower inset of Fig. 1). To account for its weak asymmetry on its high-frequency side, it has been fitted to a sum of two Gaussian functions, the main one at low frequency being about ten times larger than the second one. The extracted values for the frequency and the width of the main Gaussian contribution,

TABLE I. Frequency ν_i, decay time τ_i, corresponding FWHM γ_i, and relative normalized amplitudes $\mathcal{A}_1/\mathcal{A}_2$ [Eq. (9)] of the D_1 and D_2 modes obtained in silica glasses of density ρ from ISRS and Raman spectroscopies assuming Gaussian lineshapes.

ρ g/cm^3	Method	ν_1 cm^{-1}	τ_1 (γ_1) ps (cm^{-1})	ν_2 cm^{-1}	τ_2 (γ_2) ps (cm^{-1})	$\mathcal{A}_1/\mathcal{A}_2$
2.20	ISRS	495 ± 4	$0.55\pm0.09(19\pm3)$	605 ± 4	$0.34\pm0.04(31\pm3)$	2.25 ± 0.4
	Raman	492 ± 3		605 ± 1	$0.32\pm(33\pm2)$	
2.43	ISRS	506 ± 4	$0.44\pm0.09(24\pm5)$	609 ± 4	$0.26\pm0.04(41\pm7)$	1.2 ± 0.3
	Raman			610 ± 1	$0.24\pm(44\pm2)$	
2.63	ISRS	515 ± 4	$0.42\pm0.08(25\pm5)$	612 ± 4	$0.24\pm0.04(44\pm7)$	1.0 ± 0.3
	Raman			614 ± 1	$0.23\pm(46\pm2)$	

together with the total area of the line normalized to its v-SiO_2 value, are listed in Tables I and II. Such detailed analysis is more difficult to perform for the D_1 line because of its overlap with the R band. In particular, it is barely observable for large densities making its extraction from the spectral-domain data very imprecise. In contrast, because of their different time behavior, the R band and D_1 line can be separated in the time domain as will be discussed in Sec. IV.

IV. IMPULSIVE STIMULATED RAMAN SCATTERING

The probe transmission change $\Delta T/T$ measured on v-SiO_2 in function of the pump-probe delay t_D is shown in Fig. 3(a) (inset). Around zero delay, the signal exhibits a fast transient ascribed to coupling of the pump and probe pulses through the noninstantaneous part of the nonlinear third order susceptibility of the glass.[41–44] It is followed by weak oscillations of $\Delta T/T$ with clearly observable beating [Fig. 3(a)]. Similar results are obtained with the densified samples [Figs. 3(b) and 3(c)]. In both normal and densified silica these oscillations are associated with coherent excitation and detection of the D_1 and D_2 ring modes.[18]

This is confirmed by comparison of the spectral and time-domain data. Owing to the nonlinear coupling of the pump and probe pulses near $t_D=0$, the vibrational response can only be analyzed for time delays t_D larger than about 50 fs. Performing fast Fourier transformation (FFT) of the data beyond the cut-off time $t_c=50$ fs in v-SiO_2, only a weak contribution of the R band is observed, the FFT data being dominated by the D_1 and D_2 modes [Fig. 4(a)].[18] This is a consequence of the fast decay of the contribution of the inhomogenously broadened R band with a characteristic time reflecting its width (Sec. II). It is confirmed by the good

TABLE II. Evolution of the D_1 and D_2 normalized amplitude [Eq. (9)] upon densification obtained from time-domain and Raman data.

	D_1		D_2	
Ratio	ISRS	Raman	ISRS	Raman
$\mathcal{A}_i^{2.43}/\mathcal{A}_i^{2.20}$	1.1 ± 0.2		2.3 ± 0.4	2.5 ± 0.2
$\mathcal{A}_i^{2.63}/\mathcal{A}_i^{2.20}$	1.5 ± 0.3		4.0 ± 0.8	3.5 ± 0.3

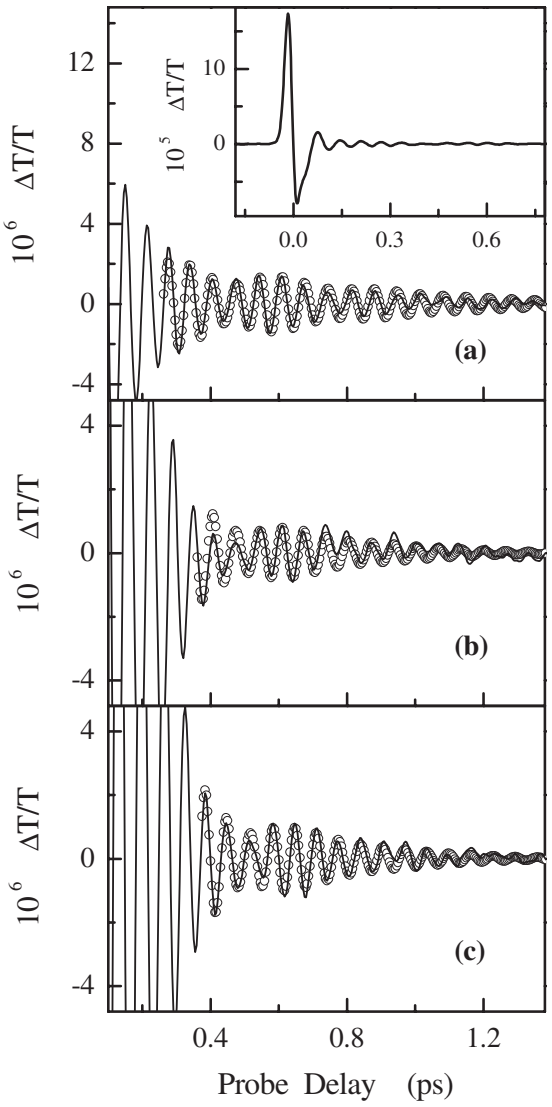

FIG. 3. Time dependence of the oscillatory part of the transmission change $\Delta T/T$ measured in normal (a) and densified vitreous SiO_2 of $\rho=2.43$ g/cm^3 (b) and $\rho=2.63$ g/cm^3 (c) for the same pump and probe wavelengths, $\lambda_{IR}\approx860$ nm. The Gaussian fits are shown for $t_c=200$, 300, and 310 fs, respectively. The inset shows the full transmission change $\Delta T/T$ measured in normal density silica.

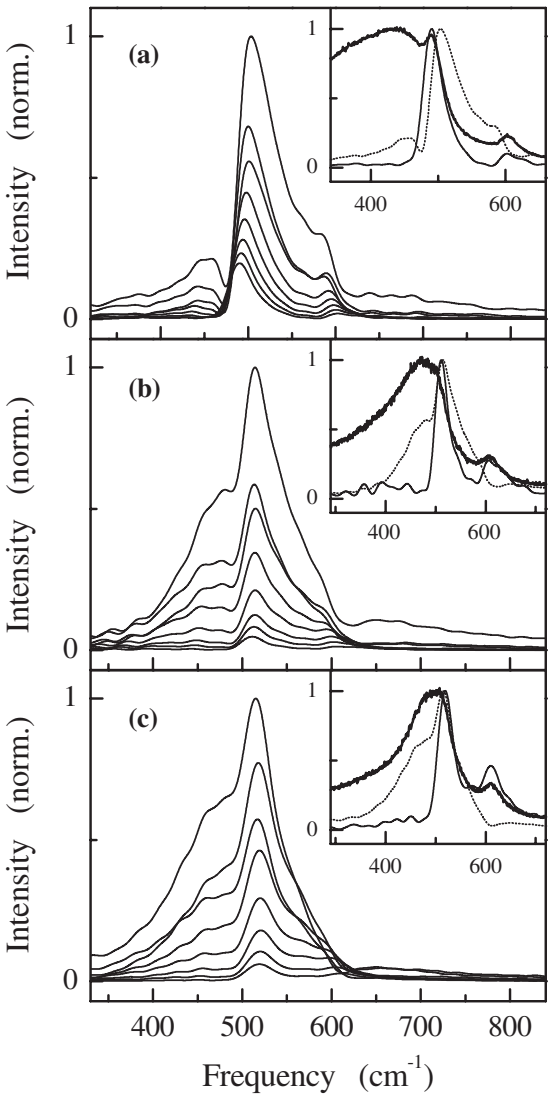

FIG. 4. Fourier transforms of the time-domain signal $\Delta T/T$ obtained in normal (a) and densified vitreous SiO_2 of $\rho=2.43$ g/cm^3 (b) and $\rho=2.63$ g/cm^3 (c) for $t_c=90$,110, 125, 140, 175, 210, 240, and 275 fs. The insets show Raman spectra (full line) and the Fourier transforms of $\Delta T/T$ for $t_c=90$ fs (dotted line) and 275 fs (thin full line); the amplitudes of the data have been normalized.

agreement between the measured $\Delta T/T$ oscillations and the time-domain signal computed from Fourier transformation of the Raman spectrum [Fig. 5(a)]. Similar behavior is observed on the densified samples, however with an increased contribution of the R band [Figs. 4(b) and 4(c)]. In particular, it lasts over a longer time scale indicating a slower dephasing, in agreement with its narrowing in the Raman spectra (Fig. 1). Selecting the long delay signal, i.e., increasing t_c above about 300 and 400 fs in v-SiO_2 and d-SiO_2, respectively, the R-band contribution can be almost suppressed, allowing for a selective observation of the slowly dephasing D_1 and D_2 modes.

To further analyze the contribution of the R band and test the possible impact of its spectral asymmetry on the long delay signal, we computed its time-domain contribution from

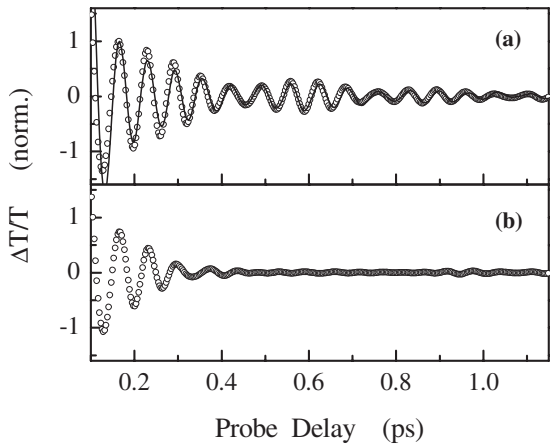

FIG. 5. (a) Oscillating part of the measured $\Delta T/T$ signal (full line) and Fourier-transform of the normalized Raman spectrum (open points) after 100 fs. (b) Fourier transform of the reduced Raman spectrum after subtraction of the D_1 and D_2 mode contributions.

the spectrum. In v-SiO_2, where the D_1 and D_2 contributions can be estimated and subtracted from the measured Raman spectrum, Fourier transformation of this modified spectrum shows large short time-delay oscillations that quickly damp [Fig. 5(b)]. After $t_D \approx 300$ fs, their amplitude is much smaller than for the time-domain signal computed from the full Raman spectra and observed experimentally [Fig. 5(a)]. This confirms that the R band significantly contributes to the short time-domain signal ($t_D \leq 300$ fs in v-SiO_2).

The properties of the D_1 and D_2 modes are thus extracted by fitting the long delay oscillating part of the signal assuming contributions from only two lines. Following Raman studies of the D_2 line, we assume Gaussian lineshapes with central frequencies $\nu_i=\omega_i/2\pi$ and decay times τ_i, i.e., use the response function (8) with $i=1,2$. As expected for nonresonant impulsive Raman-scattering experiments, cosine-type oscillations are observed. The parameters are found in Table I together with the FWHM γ_i inferred from τ_i (Sec. II). The slight blueshift of both lines upon densification is in excellent agreement with the present Raman data (Fig. 4) and previously reported ones.[45] The decay time of the oscillations decreases in the densified samples by about the same amount for the two modes (Table I). This dependence is in excellent agreement with Raman measurements for D_2 (Table I). For the D_1 mode, it is precisely determined here for the first time in densified samples.

The amplitude $\mathcal{A}_2$ is found to strongly increase with density, by a factor of about 4 from $\rho=2.20$ to 2.63 g/cm^3, almost linearly with density. This behavior is consistent with that deduced from the Raman data (Table II), confirming the reliability of the parameters extracted from the time-domain analysis. The same analysis performed on the D_1 line shows that, in contrast to $\mathcal{A}_2$, $\mathcal{A}_1$ only increases upon densification by about 50% (Table II). The clear observation of the D_1 line permits extraction of the relative mode amplitude, $\mathcal{A}_1/\mathcal{A}_2$, in each sample. However, its value in a given sample has to be used with care since the limited duration of the pump and probe pulses (i.e., their limited spectral content) can reduce

their coupling with the higher frequency mode [excitation function term in Eq. (2)]. This frequency filtering can lead to an overestimate of $\mathcal{A}_1/\mathcal{A}_2$. As the D_1 and D_2 frequencies only weakly change with density, this effect is similar in all the samples and the relative variation of $\mathcal{A}_1/\mathcal{A}_2$ is directly comparable. A decrease by a factor of about 2 from ρ =2.20 to 2.63 g/cm^3 is observed (Table I).

V. DISCUSSION: CONCENTRATION OF RINGS IN *d*-SiO_2

Silica glass has a very open network structure with a relatively small density of SiO_2 units per unit volume compared, e.g., to GeO_2. Taking for the volume occupied by a $SiO_{4/2}$ unit that of the sphere whose radius equals the main bond length (Si-O or Ge-O), the density within the sphere is $\rho^s_{SiO_{4/2}}$=5.73 g/cm^3 and $\rho^s_{GeO_{4/2}}$=7.89 g/cm^3. Dividing the glass density by these numbers gives the volume fraction occupied by the sphere, and its complement to one is the free space fraction V^f for each glass. We find $V^f_{GeO_2}$=54%, while $V^f_{SiO_2}$=62% for normal silica. For densified silica with ρ =2.63 g/cm^3 one finds $V^f_{d-SiO_2}$=54% like in normal GeO_2. This emphasizes that the free space is significantly higher in *v*-SiO_2 compared to GeO_2. It is also much higher than the 36% expected for random close packing of hard spheres. The main effect of densification in *v*-SiO_2 is to fill some of the free space by puckering the ring network. This happens by reducing the Si-O-Si angles, leaving the SiO_4 tetrahedra almost unchanged.[27] A direct consequence of this puckering is an average hardening of the structure which leads to a relatively large increase of the elastic constants.[46] Densified silicas of the same density may also have different structural properties depending on the pressure-temperature cycle as indicated from shock-wave experiments.[47] The permanent densification results from new bondings in the network, and the release of the pressure (and/or temperature) in a new distribution of local strains. These local modifications should affect the ring statistics that, for small rings, should translates into changes in the area of the D_1 and D_2 Raman lines. However, quantitative estimates of the evolution of the ring concentration from the spectral strength must take into account other mechanisms altering both the vibrational frequencies and the light-vibration coupling upon densification. These might depend on, e.g., the Si-O-Si bond angles or on a possible redistribution of the Raman-active modes.[9] Such effects are probably at the origin of the large modifications of the R band, which corresponds to O-bending motions of large $(\text{-Si-O-})_n$ structures with $n>4$. The merging of the R band and D_1 component in the densified samples (Fig. 1) is not necessarily associated to a modification of the ring statistics with an increase in the number of five and four-membered structures. The spectral change can to a large part be explained by a frequency shift of the Si-O-Si bending vibrations, as puckering always reduces the angle θ thereby increasing the vibrational frequency. This is supported by the fact that the frequency increase in the R band correlates with the intensity increase related to the decrease in θ, as discussed in Sec. III.

The fraction of oxygen atoms in small rings, estimated in *v*-SiO_2 from numerical simulations is 0.22% for the three-membered structures and 0.36% for the four-membered ones.[8] The latter corresponds to the most probable value, but it has an upper limit of 1%. Multiplying these numbers by 2/3 and 2/4, respectively, yields the concentration of rings (in %) per SiO_2 unit (or identically per $SiO_{4/2}$ tetrahedron). Owing to their very low concentration, about 1 per 670 SiO_2 units for n=3 (~0.15%) and 1 per 550 SiO_2 units for n=4 (~0.18%), these structures do not share Si atom and can be considered as independent scatterers. Moreover, breathing motions of rings mainly involve oxygen atoms and hence weakly couple to the network. Therefore, the Raman activity of these modes is directly proportional to both the number of rings and their coupling-to-light coefficient. Regarding the latter, one cannot expect that the angle θ will vary much with density in the three-membered rings, which are extremely rigid. Indeed, the relative frequency shift of the n=3 ring mode is much weaker than that of n=4, as shown in Fig. 6(b). Moreover, the Raman depolarization ratio of the D_2 line, I_{VH}/I_{VV}=1/17, is constant in our three glasses, suggesting again that the compression only weakly affects the three-membered structures. The associated puckering of the ring structure leads to an increase of the coupling-to-light Raman coefficient through the reduction of the angle θ.[8] However, the measured relative frequency shifts for both the D_1 and D_2 bands, ~4% and ~1.3%, respectively, for 20% densification, are very small compared to the increase of their corresponding spectral strength, ~50% and ~350%. In addition, the frequency variation is smaller for D_2 which exhibits the

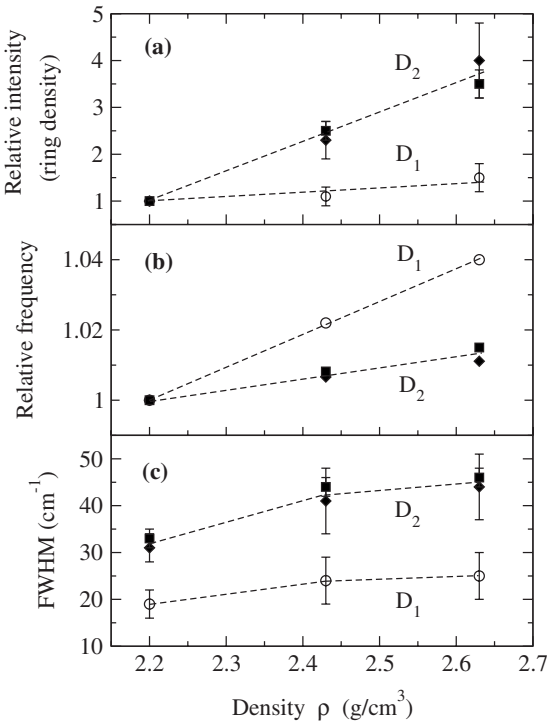

FIG. 6. (a) Increase in small rings in permanently densified silica, (b) frequency shifts of the D_1 and D_2 bands in *d*-SiO_2 relative to normal silica, and (c) variation in the FWHM upon densification. The open circles and filled diamonds corresponds to ISRS experiment results for D_1 and D_2, respectively, and the filled squares to the Raman ones for D_2.

strongest intensity increase. This definitely shows that the puckering of the small rings upon densification cannot account for the very strong increase of their spectral strength [Fig. 6(a)]. Therefore, the relative evolution of the ISRS amplitude and normalized Raman area for the D_1 and D_2 modes (Table II) provides a way to estimate the ring fraction in the permanently densified glasses.

The ring density of densified silicas relative to the value in v-SiO_2 is shown in Fig. 6(a). Within the experimental uncertainties, the small ring concentration increases linearly with silica density ρ. Three-membered rings being denser than four-membered ones, their larger concentration increase is consistent with compaction. Presumably, some fourfold rings transform into three-membered ones, an effect compensated by the transformation of five membered rings to four-membered ones, leading to an overall weak increase in the concentration of the latter. For large silica density $\rho = 2.63$ g/cm^3, we thus estimate that there is 1 per 190 ± 35 SiO_2 threefold rings compared to 1 per 380 ± 70 SiO_2 for the fourfold ones.

The widths and frequency shifts of the D_1 and D_2 lines behave differently. While for D_1 ($n=4$) the frequency changes appreciably with densification, the spectral width remains small. It increases by $\Delta\gamma_1 \simeq 6$ cm^{-1} from $\rho=2.2$ to $\rho=2.63$ g/cm^3, which is well below the corresponding frequency shift $\Delta\nu_1=20$ cm^{-1}. The opposite happens for D_2, with an increase in width $\Delta\gamma_2=13$ cm^{-1} which is larger than the related shift $\Delta\nu_2=9$ cm^{-1}. This suggests that the $n=4$ rings can pucker upon densification, which changes the angles θ but releases local stresses and therefore leaves the rings close to an equilibrium situation. The matter is different for $n=3$ rings, which hardly puckers and therefore are subject to stronger random stresses that produce a larger $\Delta\gamma$. It is also worth noting that the overlap of the D_1 line with the R band does not translates into a strong D_1 broadening in d-SiO_2, confirming the decoupling of the breathing vibrations of small ring to the rest of the network.

Finally, the slope of the frequency dependence of D_1 and D_2 upon densification in our silica glasses are significantly different to those observed on other permanently densified samples.[40,47] This confirms that the structure of densified silicas depends on the densification protocol in the densified samples.

VI. CONCLUSION

The vibrational modes of permanently densified vitreous silica has been studied by spontaneous Raman and impulsive-stimulated Raman scattering. We have focused on comparing the results of the two experimental methods in the spectral region of the D_1 and D_2 ring modes. Special care has been taken to perform measurements in similar conditions in the different samples making possible comparison of their time- or spectral-domain responses. The reliability of this approach has been checked on the D_2 line. The frequency, linewidth, and relative amplitude obtained using the two techniques are in excellent agreement. It was possible to follow the evolution of the D_1 line upon densification in the time domain, as its spectrum can be separated from the broad R band which overlaps it in spontaneous Raman studies. This allows the extraction of both D_1 and D_2 ring-mode characteristics, which are observed simultaneously in the time domain.

The increase in the relative frequency shifts is quite small and mostly relates to the reduction in the Si-O-Si angle θ in rings upon densification. The widths increase are associated to an increase of the distribution of both the Si-O-Si angle and the stresses of the ring structures. The denser structures ($n=3$) being more rigid are subject to stronger random stresses. Relative ring-mode amplitudes mostly reflect the evolution of the concentration upon densification. For threefold rings, the concentration strongly increases by a factor of about 3.5 for 20% densification. A much smaller increase, by 1.5, is estimated for the fourfold rings. In both cases, the concentration of small rings remains quite small. Intensity measurements in SiO_2 also provide a way to probe the bending motions and to estimate the reduction in the average Si-O-Si bond angle θ in densified silicas. For 20% densification we find a variation $\Delta\theta \simeq 4°$ to $5°$, a value consistent with simulations. It is emphasized here that, as for the frequencies and linewidths, the evolution of the intensity of the Raman-active modes is an important but little exploited, source of information for the investigation of the local and medium range structure in glasses.

Finally these results show the complementarity of the time and spectral-domain studies. Their combination provides a powerful experimental approach that yields new data for future comparison with *ab initio* molecular-dynamics studies of glasses.

ACKNOWLEDGMENTS

The authors thank M. Arai for providing the high quality densified samples, J. L. Sauvajol for the availability of the Raman spectra, and E. Courtens for fruitful discussion.

[1] F. L. Galeener, A. J. Leadbetter, and M. W. Stringfellow, Phys. Rev. B **27**, 1052 (1983).
[2] F. L. Galeener and J. C. Mikkelsen, Phys. Rev. B **23**, 5527 (1981).
[3] F. L. Galeener, Solid State Commun. **44**, 1037 (1982); J. Non-Cryst. Solids **49**, 53 (1982).
[4] F. L. Galeener, R. A. Barrio, E. Martinez, and R. J. Elliott, Phys. Rev. Lett. **53**, 2429 (1984).
[5] F. L. Galeener and A. E. Geissberger, Phys. Rev. B **27**, 6199 (1983).
[6] A. E. Geissberger and F. L. Galeener, Phys. Rev. B **28**, 3266 (1983).
[7] A. Pasquarello and R. Car, Phys. Rev. Lett. **80**, 5145 (1998).
[8] P. Umari, X. Gonze, and A. Pasquarello, Phys. Rev. Lett. **90**,

027401 (2003).
[9] A. Rahmani, M. Benoit, and C. Benoit, Phys. Rev. B **68**, 184202 (2003).
[10] R. A. Barrio, F. L. Galeener, E. Martinez, and R. J. Elliott, Phys. Rev. B **48**, 15672 (1993).
[11] M. R. Kozlowski and S. G. Demos, Proc. SPIE **4102**, 106 (2000).
[12] S. O. Kucheyev and S. G. Demos, Appl. Phys. Lett. **82**, 3230 (2003).
[13] *Time-Resolved Vibrational Spectroscopy*, edited by A. Laubereau and M. Stockburger (Springer-Verlag, Berlin, 1985).
[14] A. Laubereau and W. Kaiser, Rev. Mod. Phys. **50**, 607 (1978).
[15] M. M. Robinson, Y. X. Yan, E. B. Gamble, L. R. Williams, J. S. Meth, and K. A. Nelson, Chem. Phys. Lett. **112**, 491 (1984).
[16] S. De Silvestri, J. G. Fujimoto, E. P. Ippen, E. B. Gamble, L. R. Williams, and K. A. Nelson, Chem. Phys. Lett. **116**, 146 (1985).
[17] M. R. Farrar, L. R. Williams, Y. X. Yan, L. T. Cheng, and K. A. Nelson, in *Utrafast Phenomena V*, edited by G. E. Flemming and A. E. Siegman (Springer-Verlag, Berlin, 1986).
[18] C. Guillon, J. Burgin, P. Langot, F. Vallée, and B. Hehlen, Appl. Phys. Lett. **86**, 081909 (2005).
[19] J. Burgin, C. Guillon, P. Langot, F. Vallée, and B. Helhen, Appl. Phys. Lett. **89**, 251913 (2006).
[20] Y.-X. Yan and K. A. Nelson, J. Chem. Phys. **87**, 6240 (1987).
[21] L. Dhar, J. A. Rogers, and K. A. Nelson, Chem. Rev. (Washington, D.C.) **94**, 157 (1994).
[22] Y.-X. Yan, J. Edward, B. Gramble, and K. A. Nelson, J. Chem. Phys. **83**, 5391 (1985).
[23] M. Hase, K. Mizoguchi, H. Harima, S. I. Nakashima, and K. Sakai, Phys. Rev. B **58**, 5448 (1998).
[24] F. Vallée and C. Flytzanis, Phys. Rev. B **46**, 13799 (1992).
[25] W. Hayes and R. Loudon, *Scattering of Light by Crystals* (Dover, New York, 1978).
[26] L. A. Woodward, *Raman Spectroscopy* (Plenum, New York, 1967).
[27] Y. Inamura, M. Arai, N. Kitamura, S. M. Bennington, and A. C. Hannon, Physica B **241-243**, 903 (1997).
[28] E. Rat, Ph.D. thesis, University Montpellier II, 1999.
[29] S. Susman, K. J. Volin, D. L. Price, M. Grimsditch, J. P. Rino, R. K. Kalia, P. Vashishta, G. Gwanmesia, Y. Wang, and R. C. Liebermann, Phys. Rev. B **43**, 1194 (1991).
[30] B. Hehlen, E. Courtens, R. Vacher, A. Yamanaka, M. Kataoka, and K. Inoue, Phys. Rev. Lett. **84**, 5355 (2000).
[31] B. Hehlen, E. Courtens, A. Yamanaka, and K. Inoue, J. Non-Cryst. Solids **307-310**, 87 (2002).
[32] F. L. Galeener, Phys. Rev. B **19**, 4292 (1979).
[33] R. Shuker and R. W. Gammon, Phys. Rev. Lett. **25**, 222 (1970).
[34] M. Matsubara, S. Ispas, and W. Kob (private communication).
[35] C. T. Kirk, Phys. Rev. B **38**, 1255 (1988).
[36] S. N. Taraskin and S. R. Elliott, Phys. Rev. B **56**, 8605 (1997).
[37] M. Wilson, P. A. Madden, M. Hemmati, and C. A. Angell, Phys. Rev. Lett. **77**, 4023 (1996).
[38] A. Perriot, D. Vandembroucq, E. Barthel, V. Martinez, L. Grosvalet, C. Martinet, and B. Champagnon, J. Am. Ceram. Soc. **89**, 596 (2006).
[39] R. J. Hemley, H. K. Mao, P. M. Bell, and B. O. Mysen, Phys. Rev. Lett. **57**, 747 (1986).
[40] G. E. Walrafen, Y. C. Chu, and M. S. Hokmabadi, J. Chem. Phys. **92**, 6987 (1990).
[41] A. Dogariu, T. Xia, D. J. Hagan, A. A. Said, E. W. Van Stryland, and N. Bloembergen, J. Opt. Soc. Am. B **14**, 796 (1997).
[42] A. Dogariu and D. J. Hagan, Opt. Express **1**, 73 (1997).
[43] P. Langot, S. Montant, and E. Freysz, Opt. Commun. **176**, 459 (2000).
[44] J. Burgin, C. Guillon, and P. Langot, Appl. Phys. Lett. **87**, 211916 (2005).
[45] C. H. Polsky, K. H. Smith, and G. H. Wolf, J. Non-Cryst. Solids **248**, 159 (1999).
[46] E. Rat, M. Foret, G. Massiera, R. Vialla, M. Arai, R. Vacher, and E. Courtens, Phys. Rev. B **72**, 214204 (2005).
[47] H. Sugiura, R. Ikeda, K. Kondo, and T. Yamadaya, J. Appl. Phys. **81**, 1651 (1997).